Molecular Neurobiology
https://doi.org/10.1007/s12035-024-04448-2

RESEARCH

tubg1 Somatic Mutants Show Tubulinopathy-Associated Neurodevelopmental Phenotypes in a Zebrafish Model

Ozge Cark[1,2,5] · Esra Katkat[1,2] · Ipek Aydogdu[1,3] · Evin Iscan[1,2] · Yavuz Oktay[1,2,4] · Gunes Ozhan[1,3]

Received: 11 May 2024 / Accepted: 19 August 2024

Abstract

Development of the multilayered cerebral cortex relies on precise orchestration of neurogenesis, neuronal migration, and differentiation, processes tightly regulated by microtubule dynamics. Mutations in tubulin superfamily genes have been associated with tubulinopathies, encompassing a spectrum of cortical malformations including microcephaly and lissencephaly. Here, we focus on γ-tubulin, a pivotal regulator of microtubule nucleation encoded by *TUBG1*. We investigate its role in brain development using a zebrafish model with somatic *tubg1* mutation, recapitulating features of TUBG1-associated tubulinopathies in patients and mouse disease models. We demonstrate that γ-tubulin deficiency disrupts neurogenesis and brain development, mirroring microcephaly phenotypes. Furthermore, we uncover a novel potential regulatory link between γ-tubulin and canonical Wnt/β-catenin signaling, with γ-tubulin deficiency impairing Wnt activity. Our findings provide insights into the pathogenesis of cortical defects and suggest that γ-tubulin could be a potential target for further research in neurodevelopmental disorders, although challenges such as mode of action, specificity, and potential side effects must be addressed.

Keywords Zebrafish · Neurodevelopmental disorder · Tubulin gamma 1 · Tubulinopathies · Wnt/β-catenin signaling

Introduction

The complex structure of the multilayered cerebral cortex is determined by three crucial steps: the birth of neurons from neural stem cells, i.e., neurogenesis, the migration of newborn neurons to proper positions, and the neuronal differentiation and building of axonal connections between correct neurons [1–3]. Due to the essential role of microtubule orchestration in these processes, mutations in genes belonging to the tubulin superfamily have been associated with complex cortical malformations commonly referred to as tubulinopathies [4, 5]. Tubulinopathies cover a wide spectrum of clinical severity and phenotypes originating from mutations in tubulin superfamily genes including *TUBA1A*, *TUBB2A*, *TUBB2B*, *TUBB3*, *TUBB5*, *TUBGCP2*, and *TUBG1*. Variants of these genes have been linked to a range of phenotypes, including microcephaly, lissencephaly, pachygyria, polymicrogyria, and schizencephaly [6–11].

γ-Tubulin is a highly conserved tubulin superfamily protein that plays a critical role in the nucleation and orchestration of microtubules across eukaryotic organisms [12]. γ-Tubulin, in contrast to α- and β-tubulins, does not participate in the assembly of microtubules. Yet, γ-tubulin cooperates with various cytoplasmic proteins to form two different complexes: the gamma-tubulin small complex (γ-TuSC) and gamma-tubulin ring complex (γ-TuRC) [13]. These complexes serve as stable scaffolds facilitating the polymerization of α- and β-tubulin dimers [14]. In eukaryotes, γ-tubulin is encoded by two genes, *TUBG1* and *TUBG2*, which exhibit

Ozge Cark and Esra Katkat contributed equally to this work.

✉ Gunes Ozhan
gunes.ozhan@ibg.edu.tr; gunesozhan@iyte.edu.tr

1 Izmir Biomedicine and Genome Center (IBG), Dokuz Eylul University Health Campus, Inciralti-Balcova 35340, Izmir, Türkiye

2 Izmir International Biomedicine and Genome Institute (IBG-Izmir), Dokuz Eylul University, Inciralti-Balcova 35340, Izmir, Türkiye

3 Department of Molecular Biology and Genetics, Izmir Institute of Technology, Urla, 35430 Izmir, Türkiye

4 Department of Medical Biology, School of Medicine, Dokuz Eylul University, Izmir 35340, Türkiye

5 Center for Regenerative Therapies at the TU Dresden, Technische Universität Dresden, 01307 Dresden, Germany

significant similarity across many species. However, their functional roles are not equivalent. *TUBG1* plays a critical role in microtubule nucleation during developmental processes, thereby influencing microtubule-dependent cellular events including mitosis, cell motility, and the formation of cell projections [15, 16]. Given the significance of these processes in cerebral cortex development, which relies on well-organized neuronal proliferation, migration, differentiation, and axonal growth, mutations in the *TUBG1* gene are strongly linked to cortical abnormalities. To date, 13 individuals exhibiting microcephaly, pachygyria, motor impairments, intellectual disabilities, and epilepsy have been associated with missense mutations in *TUBG1* [9, 11, 17, 18]. Unlike *TUBG1*, which is essential in dividing cells, *TUBG2* plays a more significant role in non-dividing, differentiated cells, particularly in neurons, contributing to neuronal differentiation and the maintenance of specialized microtubule architecture necessary for their function (16). A de novo missense variant in *TUBG2* has recently been implicated in cortical malformations, including polymicrogyria and microcephaly, potentially by altering protein interactions and cell growth (19).

Wnt/β-catenin signaling pathway, also known as the canonical Wnt pathway, plays pivotal and multifaceted roles in cortical development, orchestrating neuroectodermal patterning, the balance between neural stem cell proliferation and differentiation, axonal growth and orientation, cell polarity and motility, dendritogenesis, and synaptogenesis [20–24]. The canonical Wnt pathway acts through controlling accumulation and nuclear translocation of β-catenin, activating specific gene expression programs in a cellular context-dependent manner. Wnt ligands bind to the Wnt receptor complex composed of frizzled and LRP5/6 receptors, initiating the disassembly of the β-catenin destruction complex (Axin, APC, GSK3, CK1, PP2A) in the cytoplasm, thereby preventing β-catenin degradation and facilitating its translocation to the nucleus [25, 26]. Numerous studies have demonstrated that disrupting pathway components in vivo leads to diverse defects in neural tube formation, brain compartmentalization, neural precursor proliferation, differentiation, and migration [20, 24]. Furthermore, mutations in *WD Repeat and FYVE Domain Containing 3* (*WDFY3*) and *Assembly Factor for Spindle Microtubules* (*ASPM*) genes, which interfere with Wnt/β-catenin signaling, have been associated with human pathogenesis related to microcephaly and cortical defects [27, 28]. Thus, unraveling new components in the association of canonical Wnt signaling with neural development could provide critical insights into understanding the pathogenesis of microcephaly and cortical defects in humans.

In this study, we investigated the involvement of *tubulin gamma 1* (*tubg1*) in early brain development and examined its functional interplay with the canonical Wnt signaling pathway. To address the limitations of existing models and to provide a more comprehensive understanding of *tubg1*-associated tubulinopathies, we developed a zebrafish model with somatic generation 0 (G0) *tubg1* mutation, resulting in in vivo knockdown of γ-Tubulin 1. The zebrafish model presents several unique advantages. Its transparency allows for real-time imaging of neuronal development and migration, facilitating detailed studies of dynamic neurodevelopmental processes. Zebrafish embryos also develop rapidly and are highly amenable to genetic manipulation, enabling high-throughput genetic screening and functional analyses that are less feasible in murine models. These advantages make the zebrafish model a powerful complementary tool to existing mouse and cellular models, advancing our understanding of the molecular mechanisms underlying tubulinopathies and identifying potential therapeutic targets. Our findings reveal that somatic *tubg1* mutation disrupts neurogenesis and brain development in zebrafish, effectively mimicking the microcephaly observed in TUBG1-associated tubulinopathies. Furthermore, we showed that γ-tubulin deficiency resulted in reduced Wnt signaling activity, whereas γ-tubulin overexpression caused an increase in Wnt target genes, suggesting that γ-tubulin plays a regulatory role in Wnt/β-catenin signaling.

Materials and Methods

Zebrafish Handling and Maintenance

Zebrafish were maintained in the zebrafish facility of Izmir Biomedicine and Genome Center (IBG) under standard conditions, with a 12-h light–dark cycle at 28 °C, following the regulations set forth by the IBG Animal Care and Use Committee. All animal experiments were approved by the Animal Experiments Local Ethics Committee of the IBG (IBG-AELEC). The AB strain was utilized as the wild-type (wt) zebrafish. Tg(*7XCF-Xla.Sia*:NLS-mCherry)^{ia} transgenic zebrafish line served as a reporter of Wnt/β-catenin signaling and was outcrossed to wt fish. Embryos were sorted following previously established protocols (confined,[29]). Tg(mbp:EGFP-CAAX) transgenic zebrafish line was used as a reporter of myelinating oligodendrocytes and was used via incross [30]. Embryos obtained from natural spawnings were maintained in E3 medium until 5 days post-fertilization (dpf), after which they were transferred to the aquarium system as described previously [31]. Developmental staging was determined as previously outlined [32]. Microinjections were performed on one-cell stage embryos, with experiments conducted using embryos from multiple clutches produced simultaneously.

Cloning

The coding sequence of zebrafish *tubg1* (GenBank: CT573704.7) was amplified using cDNA derived from total RNA extracted from pooled zebrafish embryos at 24 h post-fertilization (hpf). PCR primers were designed using Primer-BLAST from the U.S. National Center for Biotechnology Information (NCBI) [33] (Table S1). To clone *tubg1-GFP* construct, a two-step PCR process was performed with a secondary primer pair containing restriction enzyme recognition sequences at 5′ end (Table S1). The forward primer was designed to include a BamHI recognition sequence and a Kozak sequence, while the reverse primer to include an EcoRI recognition sequence. Subsequently, the *tubg1* PCR product was digested with BamHI and EcoRI and ligated into an expression vector pCS2P + containing EGFP. Similarly, for the Tubg1-Flag construct cloning, a two-step PCR process was performed using a secondary primer pair containing restriction enzyme recognition sequences at 5′ end (Table S1). The forward primer was appended with a BamHI recognition sequence and a Kozak sequence, while the reverse primer was appended with a FLAG sequence and an EcoRI recognition sequence. Following PCR amplification, the *tubg1* PCR product was digested with BamHI and EcoRI and subsequently ligated into the expression vector pCS2P + .

RNA Extraction, cDNA Synthesis, and Real-Time Quantitative PCR

RNA was extracted from whole 24 hpf embryos or heads of 2.5 or 5 dpf larvae using Qiazol (Qiagen, Hilden, Germany) and purified with the miRNeasy Micro Kit (Qiagen, Hilden, Germany). Thirty embryos/larvae were pooled for each experimental group. All samples were converted to cDNA using ProtoScript II First Strand cDNA Synthesis Kit (New England BioLabs, MA, USA), according to the manufacturer's protocol. The zebrafish *ribosomal protein L13a* (*rpl13a*) gene was used as the housekeeping gene for normalization to determine relative gene expression levels. All real-time quantitative PCR (RT-qPCR) primers were designed using Primer-BLAST from the NCBI (Table S2). RT-qPCR was performed in triplicate using GoTaq qPCR Master Mix (Promega, Madison, WI, USA) on an Applied Biosystems 7500 Fast Real-Time PCR machine (Applied Biosystems, MA, USA). The data were analyzed as described previously [34]. Graphs were generated by using the GraphPad Prism 8 software (Graphpad Software Inc., CA, USA). Statistical significance was evaluated by a one-sample *t*-test. The values represent the mean ± standard deviation (SD) of three samples.

RNA Probe Synthesis and Whole-Mount In Situ *Hybridization*

For the PCR-based approach for the preparation of RNA probes, specific primers for cDNA sequences of target mRNAs were designed using Primer-BLAST from NCBI [33] (Table S3). The promoter sequence of T7 RNA polymerase was added to the 5′ end of each reverse primer. Primer pairs were utilized to generate templates for RNA probe synthesis via PCR from 5 dpf zebrafish larval cDNA. Subsequently, PCR-based templates were purified using NucleoSpin Gel and PCR Clean-up Kit (Macherey–Nagel, Duren, Germany). Digoxigenin (DIG)-labeled antisense RNA probes were synthesized by in vitro transcription using DIG RNA labeling mix (Merck & Co., Inc., NJ, USA) and T7 RNA polymerase kit (Thermo Fisher Scientific, MA, USA) following the manufacturer's protocol. The synthesized DIG-labeled antisense RNA probes were purified using the RNA Clean and Concentrator-25 kit (Zymo Research, CA, USA). For whole-mount in situ hybridization (WMISH), zebrafish larvae were fixed at 5 dpf in 4% PFA overnight. WMISH was conducted using antisense probes for *tubg1*, *prox1a*, *mCherry*, *mag*, *calb2a*, *gabra4*, egr2a, and *fgf3* as described previously [35].

Capped Sense mRNA Synthesis and Microinjection

Initially, 5 µg of each plasmid containing coding sequences *Tubg1-GFP* and *GFP* (control) was linearized using XbaI restriction enzyme (Thermo Fisher Scientific, Waltham, MA, USA) for 5 h. Subsequently, the linearized plasmids were purified using NucleoSpin Gel and PCR Clean-up Kit (Macherey–Nagel, Duren, Germany). Capped sense RNAs were synthesized in vitro using mMessage mMachine SP6 Transcription Kit (Thermo Fisher Scientific, MA, USA) following the protocol outlined in kit user manual. The synthesized mRNAs were purified using the RNA Clean and Concentrator-25 (Zymo Research, CA, USA).

CRISPR/Cas9-Mediated Gene ED diting

The coding sequence of zebrafish *tubg1* was divided into five equal segments and four single guide RNAs (sgRNAs) were designed to target the first four segments, as described previously [36]. Oligonucleotide templates for the target-specific forward gRNA primers, containing a T7 promoter and encoding the standard sgRNA chimeric scaffold, were designed (Table S4). These oligonucleotide templates were dissolved in distilled water to create a 100 mM stock solution. Ten microliters of each forward and reverse oligonucleotides was mixed with 180-µL distilled water and annealed, as described previously, using Phusion High-Fidelity DNA Polymerase (New England Biolabs, MA, USA). The

resulting annealed double-stranded oligonucleotide templates were purified and eluted in distilled water following the column purification protocol provided by the NucleoSpin Gel and PCR Clean-up Kit (Macherey–Nagel, Duren, Germany). sgRNAs were synthesized in vitro from the annealed oligonucleotide templates (1000 ng per reaction) using the HiScribe™ T7 Quick High Yield RNA Synthesis Kit (New England Biolabs, MA, USA), as described previously [36]. The resulting RNA was purified using the RNA Clean and Concentrator-25 (Zymo Research, CA, USA). Guide-it Recombinant Cas9 protein (Takara Bio Inc, Shiga, Japan) was mixed at a 1:1 ratio (750 ng/750 ng) with the sgRNA solution to form Cas9/sgRNA complexes. A 0.05% phenol red dye was included for visualization during injections. When multiple sgRNAs, ranging from two to four, were combined, the total sgRNA concentration was maintained at 750 ng/µl, ensuring that the concentration of each sgRNA was 187.5 ng/µl. The Cas9 protein-sgRNA mixture was incubated at room temperature (RT) for 5 min and then kept on ice during microinjection, which was performed by injecting 2 nl of the mixture into the cytoplasm of one-cell stage zebrafish embryos.

Whole-Mount Immunofluorescence Staining of Zebrafish Larvae

The immunofluorescence staining was performed as described previously (37). Larvae were fixed in 4% paraformaldehyde (PFA) in 1X PBS overnight at 4 °C and washed with 1 × PDT (1X PBST, 0.3% Triton-X, 1% DMSO). Permeabilization was conducted by treating the fixed larvae with ice-cold acetone at − 20 °C for 7 min, followed by blocking for 1 h in a buffer containing 10% bovine serum albumin, 1% DMSO, 0.3% Triton-X, and 1.5% (v/v) goat serum. Larvae were incubated with the primary antibody overnight at 4 °C. The next day, larvae were washed several times with PBS/0.1% Triton and incubated with the secondary antibody for 2 h at RT. After washing with PBS/0.1% Triton, larvae were mounted in 80% glycerol between two coverslips and stored at 4 °C. The antibodies used were rabbit anti-GFP (#2956, Cell Signaling Technology, MA, USA), mouse anti-HuC/HuD Antibody (#A-21271, Thermo Fisher Scientific, MA, USA), and fluorescein (FITC) donkey anti-rabbit immunoglobulin G (IgG) (711–096-152, Jackson Immunoresearch Laboratories, PA, USA). Nuclear staining was carried out using 4′,6-diamidino-2-phenylindole (DAPI; 4083S, Cell Signaling Technology, MA, USA). Larvae were imaged using a Zeiss LSM880 fluorescence confocal microscopy (Carl Zeiss AG, Jena, Germany). Confocal images were captured with a 25X objective lens using the z-stack function with a 10-µm interval between each slice. For fluorescence intensity measurement in the Tg(mbp:EGFP-CAAX) transgenic line, the regions of interest were selected at the midline periphery of the ventral hindbrain in each embryo. Fluorescence intensity measurements were also performed on HUC/D-stained 5 dpf embryo samples, specifically for the two hemispheres of the telencephalon in each larvae. Intensity measurements were calculated after converting each image to an 8-bit format. Standard brightness and contrast settings were applied to all images, and the regions of interest (ROI) were measured using integrated density in FIJI (National Institutes of Health, NY, USA).

Western Blotting

The larval tissues were homogenized in RIPA lysis buffer and centrifuged at maximum speed for 30 min at 4 °C. The resulting supernatants were collected and mixed with 5X SDS loading buffer. Subsequently, the samples were subjected to electrophoresis on a 12% acrylamide-bis acrylamide gel and transferred onto a nitrocellulose membrane for western blot analysis. Blocking was performed using 5% BSA for 1 h at RT. The samples were then incubated overnight at 4 °C with the following primary antibodies: mouse anti-gamma Tubulin (#GTX11316, GeneTex Inc., CA, USA) and rabbit anti-β-actin (#4967, Cell Signaling Technology, MA, USA). Secondary antibodies were donkey anti-rabbit IgG horseradish peroxidase (HRP)–linked LICOR IRDye 800CW (LI-COR Biosciences, NE, USA) and goat anti-rabbit IgG DyLight™ 800 4X PEG Conjugate (#5151 Cell Signaling Technology, MA, USA).

Co-immunoprecipitation

To analyze the interaction between Tubg1 and Axin proteins, HEK293-T cells were seeded in 10-cm cell culture plates and transfected with 5 µg of each plasmid containing the coding sequences for *Tubg1-Flag* and *GFP*. After 48 h, the cells were washed with ice-cold 1X PBS and lysed using NOP buffer (10 Mm Hepes,150 Mm NaCl, 2 mM EDTA, 1%NP40, 10% glycerol) supplemented with protease and phosphatase inhibitors. Protein concentrations were determined using the Pierce BCA Protein Assay Kit following the manufacturer's instructions (Thermo Fisher Scientific, MA, USA). For co-immunoprecipitation, total cell lysates were precipitated using the Dynabead™ Protein G Co-Immunoprecipitation Kit (Thermo Fisher Scientific, MA, USA) according to the manufacturer's instructions. Dynabeads and protein complexes were separately incubated with a goat anti-Axin antibody (#sc-8567, TX, USA) and the bound proteins were subsequently analyzed by western blotting.

Data Analysis and Statistics

Each experiment was performed at least three times. All quantitative data were tested for normality using Shapiro–Wilk's *W*-test and followed by the application of appropriate statistical tests, including unpaired *t*-test and Mann–Whitney *U* test. Categorical variables were analyzed using a chi-square test followed by a post hoc multiple comparison test with Bonferroni correction. Statistical significance was determined based on a *p* value below 0.05. ($*p<0.05, **p<0.01, ***p<0.001$, and $****p<0.0001$). Graphs were generated using GraphPad Prism 8.

Results

A G0 Somatic Mutation in *tubg1* Results in a Phenotype Resembling Microcephaly in Zebrafish

The zebrafish genome contains a single *tubg1* ortholog encoding for a protein that shares a remarkable 98.00% identity with the human TUBG1 (γ-tubulin) protein. To explore the effects of *tubg1* loss of function in vivo, we generated a zebrafish knockdown model using CRISPR/Cas9 genome editing technology. Segmentation of the zebrafish *tubg1* coding sequence into five equal parts facilitated the design of four sgRNAs targeting the initial four segments, ensuring effective disruption of the gene function, as previously outlined [36]. Injection of sgRNA and Cas9 protein into zebrafish embryos efficiently induced biallelic mutations in the targeted genes across a large fraction of cells, resulting in loss-of-function phenotypes in G0 zebrafish. Due to the lethality of *tubg1* (−/−) mutations in most animals, including zebrafish, gRNA-injected zebrafish larvae served as a G0 loss-of-function model, hereafter referred to as "crispants." Phenotypic analysis showed that *tubg1* crispants started to exhibit subtle microcephaly features by 2.5 dpf (60 hpf) (Fig. 1A). By 5 dpf, the crispants displayed significantly smaller heads and eyes compared to control gRNA-injected larvae, with no detectable alterations in body length (Fig. 1B). Next, we assessed the outcome of tubg1loss-of-functionby examining the expression of glial, neuronal and apoptotic marker genes. RT-qPCR revealed that the expression of the glial cell marker *gfap* and the neuronal progenitor cell markers *nestin* and *sox2* did not change significantly, indicating that the overall population of these cells remains unaffected in crispants. Similarly, the expression levels of pro-apoptotic and anti-apoptotic genes remained unchanged, suggesting that the induction of apoptosis is not a contributing factor to the observed phenotypes (Fig. 1C). We also found Tubg1 protein level to be reduced in *tubg1* crispants at 5 dpf (Fig. 1D). These findings suggest that while the

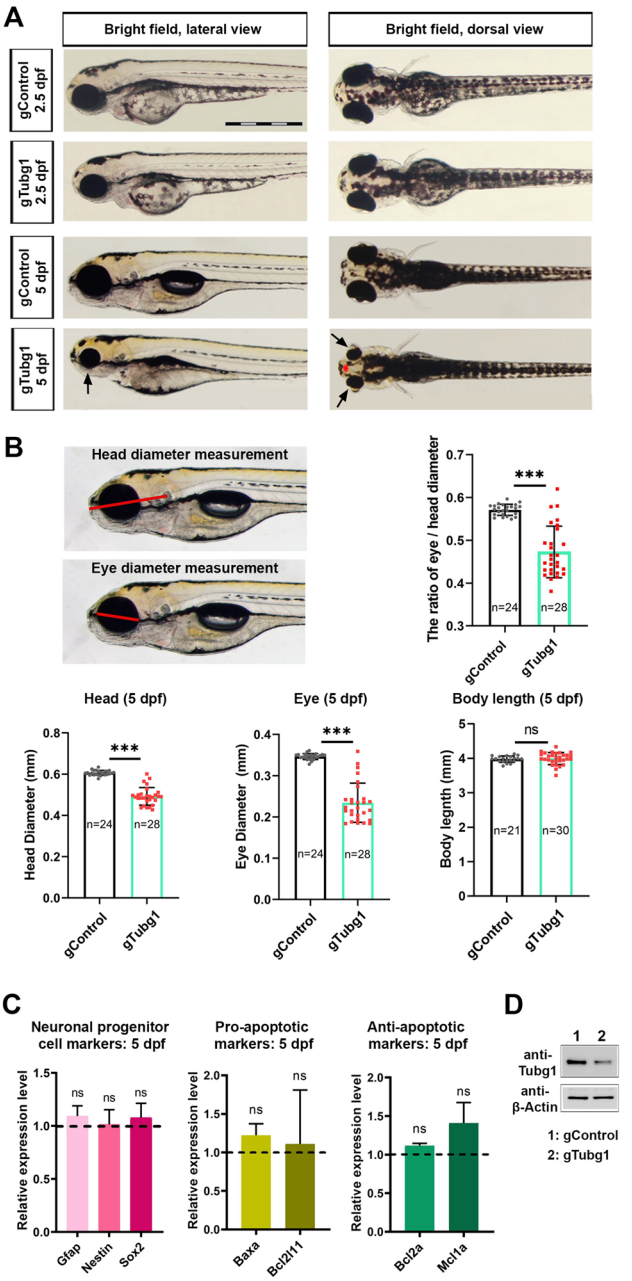

Fig. 1 A G0 somatic mutation in *tubg1* results in a phenotype resembling microcephaly in zebrafish. **A** Bright-field images of zebrafish larvae show that the effects of somatic *tubg1* mutation on neurodevelopment become slightly visible after 2.5 dpf and predominantly evident at 5 dpf. At 5 dpf, there is a significant reduction in head area (red label) and eye size (arrows). **B** Quantification of head size, eye size, and body length in *tubg1* crispants at 5 dpf. Heads and eyes, but not body length, are significantly smaller in crispants compared to control gRNA-injected larvae (unpaired *t*-test or Mann–Whitney *U* test $***p<0.001$). **C** RT-qPCR on heads of *tubg1* crispants shows no alteration in expression of glial cell, neuronal progenitor, and pro-apoptotic and anti-apoptotic marker genes at 5 dpf. The relative expression levels of the genes were normalized to *rpl13a*. The fold changes in gene expression were then normalized to the control condition, which was set as the baseline with an expression level of 1. Statistical significance was evaluated by a one-sample *t*-test. $*p<0.05$, $**p<0.01$, $***p<0.001$, and ns non-significant. **D** Western blot of larval heads for Tubg1 and β-actin (loading control) displays reduced Tubg1 expression in *tubg1* crispants at 5 dpf. gControl, scrambled gRNAs; gTubg1, *tubg1* gRNAs (*tubg1* crispant). Error bars represent ± standard deviation (SD, $n=3$). Scale bar 1 mm

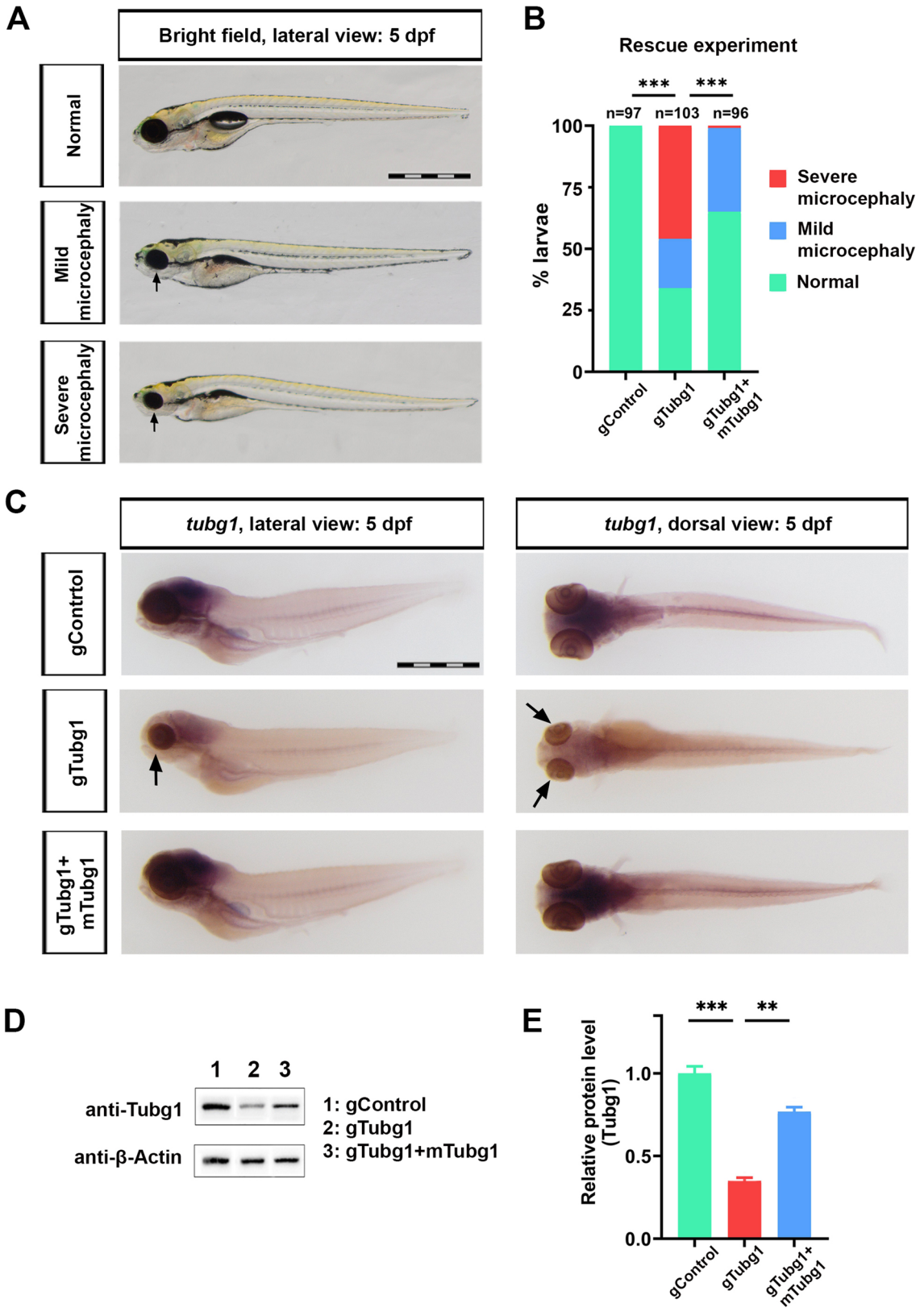
A
Bright field, lateral view: 5 dpf
Normal
Mild microcephaly
Severe microcephaly
B
Rescue experiment
***
***
n=97
n=103
n=96
100
75
50
25
0
% larvae
Severe microcephaly
Mild microcephaly
Normal
gControl
gTubg1
gTubg1+ mTubg1
C
tubg1, lateral view: 5 dpf
tubg1, dorsal view: 5 dpf
gContrtol
gTubg1
gTubg1+ mTubg1
D
1 2 3
anti-Tubg1
anti-β-Actin
1: gControl
2: gTubg1
3: gTubg1+mTubg1
E
***
**
Relative protein level (Tubg1)
1.0
0.5
0.0
gControl
gTubg1
gTubg1+ mTubg1

◂**Fig. 2** *tubg1* mRNA overexpression rescues the microcephaly phenotype in *tubg1* crispants. **A** Bright-field images of zebrafish larvae at 5 dpf showing the normal larvae, larvae having mild microcephaly, and larvae having severe microcephaly. The arrows indicate the reduction in eye size. **B** Distribution of larval phenotypes in control, crispant, and rescue groups based on their craniofacial development at 5 dpf (gControl $n=97$, gTubg1 $n=103$, gTubg1 + mTubg1 $n=96$ (chi-square test followed by post hoc analysis with Bonferroni correction $^{***}p<0.001$). Co-injection of *tubg1* mRNA effectively rescues the effects of somatic *tubg1* mutation on neurodevelopment. **C** Whole-mount in situ hybridization for *tubg1* at 5 dpf shows a decrease and rescue of *tubg1* mRNA expression in crispant and rescue groups, respectively. **D** Western blot of larval heads for Tubg1 and β-actin (loading control) at 5 dpf shows a decrease and rescue of Tubg1 expression in crispant and rescue groups, respectively **E** Quantification of the average relative density ratios of Tubg1 to β-actin from three independent western blotting experiments shown in **D**. gControl, scrambled gRNAs; gTubg1, *tubg1* gRNAs (*tubg1* crispant); mTubg1, *tubg1* mRNA; gTubg1 + mTubg1, rescue group. Statistical significance was evaluated using an ANOVA. $^{**}p<0.01$ and $^{***}p<0.001$. Error bars represent ± standard deviation (SD, $n=3$). Scale bars 1 mm

targeted mutagenesis of *tubg1* leads to a noticeable reduction in head and eye size by 5 dpf, it does not significantly alter the populations of glial cells or neuronal progenitors, nor does it affect the balance between cell survival and apoptosis. This indicates that the microcephaly observed in *tubg1* crispants is likely due to the specific role of *tubg1* in neural development, rather than a general reduction in neural progenitor cells or an increase in cell death.

tubg1 mRNA Overexpression Rescues the Microcephaly Phenotype in tubg1 Crispants

To elucidate the potential of *tubg1* mRNA in restoring the developmental defects in the *tubg1* crispants, we co-administered *tubg1* mRNA with *tubg1* gRNAs + Cas9 mix to one-cell stage embryos. We classified larvae into two distinct phenotypes based on their craniofacial development: those exhibiting typical development and those displaying mild to severe head developmental defects. As previously demonstrated, *tubg1* crispants exhibited severe head and ocular developmental defects, leading to severe or mild microcephaly in 66% of the larvae (Fig. 2A, B). Co-injection of *tubg1* mRNA into *tubg1* crispants resulted in complete rescue of the developmental defects in 33% of the larvae and almost nearly abolished severe microcephaly. Moreover, we performed WMISH to examine changes in *tubg1* mRNA expression. *tubg1* mRNA levels dramatically decreased in *tubg1* crispants but were restored to control levels following *tubg1* mRNA co-injection (Fig. 2C). Western blotting for Tubg1 in crispants further confirmed the knockdown of Tubg1 expression at the protein level and demonstrated restoration of its expression through *tubg1* mRNA co-injection (Fig. 2D, E). These findings indicate that co-injection of *tubg1* mRNA into *tubg1* crispants efficiently rescued developmental defects and reduced the incidence of microcephaly, accompanied by the restoration of *tubg1* expression at the mRNA and protein levels.

Somatic *tubg1* Mutation Results in Impaired Neurogenesis and Brain Development

To assess neurological defects, we first conducted RT-qPCR analyses in *tubg1* crispants at 2.5 and 5 dpf. Tissue samples were collected from zebrafish larval heads for the neurogenesis-related genes *neuronal differentiation 1* (*neuroD1*) and *ELAV like neuron-specific RNA binding protein 3* (*elavl3*). NeuroD1 is a marker for differentiating neurons and is primarily expressed in the developing forebrain, midbrain, and hindbrain. Elavl3, also known as HuC, is expressed in post-mitotic neurons across various brain regions, including the forebrain, midbrain, and hindbrain. The relative expression levels of the genes remained unchanged at 2.5 dpf, whereas a significant decrease was detectable at 5 dpf (Fig. 3A). Furthermore, we evaluated the expression levels and patterns of a group of mRNAs related to forebrain, midbrain, and hindbrain development using WMISH. The expression level of *prospero homeobox 1a* (*prox1a*), which is associated with neural progenitor cells, neurogenesis, and retinal development, strongly decreased in the forebrain-midbrain (diencephalic-mesencephalic) boundary and retina of the *tubg1* crispants (Fig. 3B). Prox1a is critical for the differentiation of neural progenitors in the forebrain and midbrain regions. Expression of *fibroblast growth factor 3* (*fgf3*), a gene crucial for midbrain-hindbrain boundary development, and *early growth response 2a* (*egr2a*), involved in hindbrain segmentation and patterning, were also severely reduced in *tubg1* crispants. *Gamma-aminobutyric acid type A receptor subunit alpha4* (*gabra4*) expression, encoding for the main inhibitory neurotransmitter receptor in the central nervous system (CNS) and marking the forebrain and more prominently the midbrain-hindbrain boundary, likewise dramatically decreased in the *tubg1* crispants compared to the control group [38]. *Myelin-associated glycoprotein* (*mag*), marking the oligodendrocytes in the forebrain and the midbrain-hindbrain boundary, displayed reduced expression levels in the crispants. Notably, the most dramatic reduction was observed in the expression of *calbindin 2a* (*calb2a*), marking a wide range of tissues in the developing brain including the olfactory bulb, retina, cerebellum, and hindbrain. Calb2a is involved in calcium signaling in various neuronal populations, contributing to the regulation of neuronal excitability and neurotransmitter release.

Overall, the remarkable reductions in the expression levels of neurogenesis-related genes in *tubg1* crispants indicate widespread disruption in neurodevelopmental processes and brain development. These findings suggest that

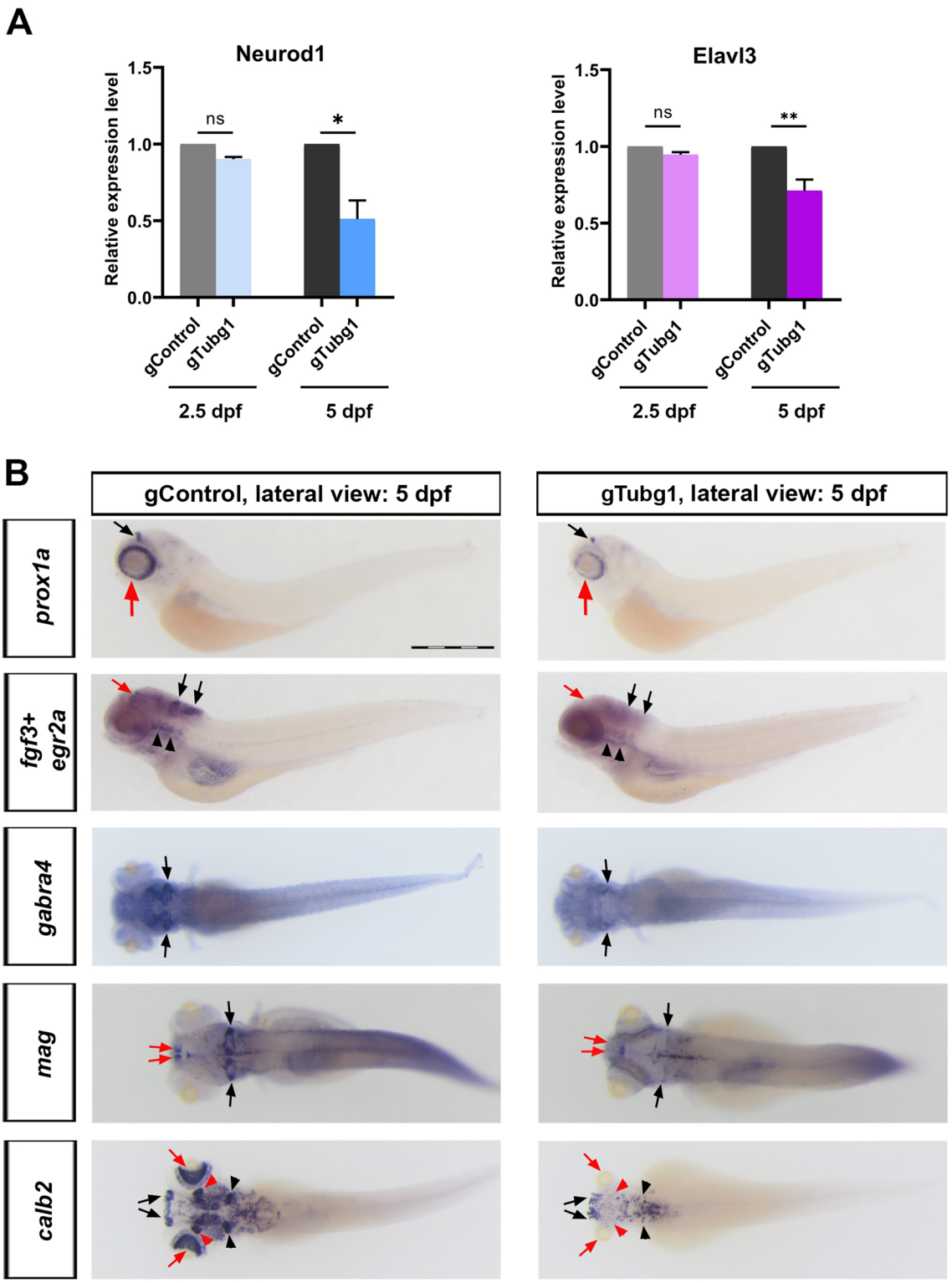

all major brain regions and a variety of neuronal populations are impacted by *tubg1* knockdown. This widespread effect aligns with the complex phenotypes observed in human patients and mouse models of *tubg1*-associated tubulinopathies, providing further insights into the critical role of γ-tubulin in brain development.

◂**Fig. 3** Somatic *tubg1* mutation results in impaired neurogenesis and brain development. **A** RT-qPCR on heads of *tubg1* crispants for *neurod1* and *elavl3* shows no change in their expression at 2.5 dpf but reveals a reduction at 5 dpf compared to the control. The relative expression levels of the genes were normalized to *rpl13a*. The fold changes in gene expression were then normalized to the control condition, which was set as the baseline with an expression level of 1. Statistical significance was evaluated by a one-sample *t*-test. $*p<0.05$, $**p<0.01$, and ns non-significant. Error bars represent ± standard deviation (SD, $n=3$). **B** Whole-mount in situ hybridizations for *prox1a* ($n=46$), *fgf3*+*egr2a* ($n=17$), *gabra4* ($n=23$), *mag* ($n=29$), and *calb2a* ($n=21$) at 5 dpf. Expression of *prox1a* is reduced in the diencephalic-mesencephalic boundary (black arrow) and the retina (red arrow) of the crispants. Co-reduction of *egr2a* and *fgf3* expression is noted in the tectum, midbrain (red arrow), hindbrain (black arrows), and branchial arches (arrowheads), while *gabra4* expression decreases in the forebrain and the midbrain-hindbrain boundary (arrows) of the crispants. Expression of *mag* decreases in the forebrain (red arrows) and midbrain-hindbrain boundary (arrows), whereas *calb2a* expression decreases in various cranial structures, including the olfactory bulb (black arrows), retina (red arrows), cerebellum (red arrowheads), and hindbrain (black arrowheads). gControl, scrambled gRNAs; gTubg1, *tubg1* gRNAs (*tubg1* crispant). Scale bars 1 mm

tubg1 Crispants Show Defects in Myelination and Reduction in Differentiated Neurons

By 5 dpf, neurogenesis in *tubg1* crispants was significantly impaired. To investigate the specific impact of *tubg1* loss on myelin development, we utilized the Tg(mbp:EGFP-CAAX) transgenic zebrafish line, in which EGFP is targeted to the membrane of myelin basic protein (Mbp)–expressing oligodendrocytes [30]. By performing immunofluorescence staining of EGFP protein, we found that the myelination pattern in *tubg1* crispants exhibited a notable decrease at the midline periphery of the ventral hindbrain compared to the control group (Fig. 4A). Furthermore, we observed a significant reduction in the number of differentiated neurons in the brain regions of crispants, as detected by immunofluorescence staining with the anti-HUC/D antibody, which identifies neuronal cell bodies (Fig. 4B). Specifically, we noted a remarkable reduction in staining intensity within the telencephalon region and a near-complete absence of staining in the hindbrain-midbrain boundary of *tubg1* crispants compared to controls. The HuC/D antibody labels differentiated neurons, indicating that the reduction in staining intensity reflects a decrease in the number of mature neurons. These findings suggest that the *tubg1* gene plays a crucial role in regulating the differentiation and distribution of neurons. The observed defects in myelination and the differentiation of neuronal populations provide valuable insights into its impact on neuronal development and function.

tubg1 Crispants Display Reduced Wnt/β-Catenin Signaling in the Head Regions

Wnt/β-catenin signaling is an essential signaling in self-renewal and differentiation in cortical neurogenesis during early brain development. To determine the impact of Tubg1 deficiency on canonical Wnt signaling, we first exploited a transgenic reporter of Tcf/Lef-mediated transcription, Tg(*7XCF-Xla.Sia*:NLS-mCherry)^{ia} [29]. By 5 dpf, Wnt/β-catenin signaling is primarily confined to the CNS, especially in the blood vessels of brain regions [29]. Our analysis revealed a decrease in Wnt reporter expression in *tubg1* crispants at 5 dpf (Fig. 5A). To further investigate the effect of *tubg1* deficiency on Wnt/β-catenin signaling, we quantified the expression levels of Wnt target genes *lef1* and *sp5l* in the heads of *tubg1* crispants at 2.5 dpf and 5 dpf using RT-qPCR [39, 40]. The expression of *lef1*, alongside that of *tubg1*, was significantly reduced at both time points, whereas *sp5l* expression showed a significant decrease only at 5 dpf (Fig. 5B). As a complementary approach, we examined whether *tubg1* overexpression in zebrafish induces elevated Wnt signaling activity, by assessing the expression levels of *lef1* and *sp5l* genes in the heads of zebrafish larvae injected with *tubg1* mRNA or EGFP mRNA as control. Larvae injected with mRNA displayed normal development and maintained the increased expression of *tubg1* mRNA until 5 dpf (Fig. 5C). At 2.5 dpf, *lef1* expression remained unchanged while *sp5l* expression increased. At 5dpf, both *lef1* and *sp5l* expression levels exhibited an increase caused by *tubg1* overexpression. These results together suggest that the main effect of *tubg1* on Wnt/β-catenin signaling becomes detectable by 5 dpf.

Previous studies have reported interactions between γ-tubulin and Axin, along with other proteins involved in Wnt/β-catenin signaling [41–43]. Thus, we asked whether γ-tubulin plays a regulatory role in Wnt/β-catenin signaling through its interactions with Axin, a component of the β-catenin destruction complex. Co-immunoprecipitation analysis revealed that zebrafish γ-tubulin interacts with Axin, suggesting a possible role in regulating Wnt/β-catenin signaling through this interaction (Fig. 5D). Thus, we propose that *tubg1* may act as a positive regulator of Wnt/β-catenin signaling in the brain, potentially through its interaction with Axin1.

Discussion

The tubulin superfamily plays a pivotal role in microtubule organization, which is essential for cortical development. While various tubulin-encoding genes have been associated with brain malformations such as microcephaly, lissencephaly, and pachygyria and clinical data have been amassed,

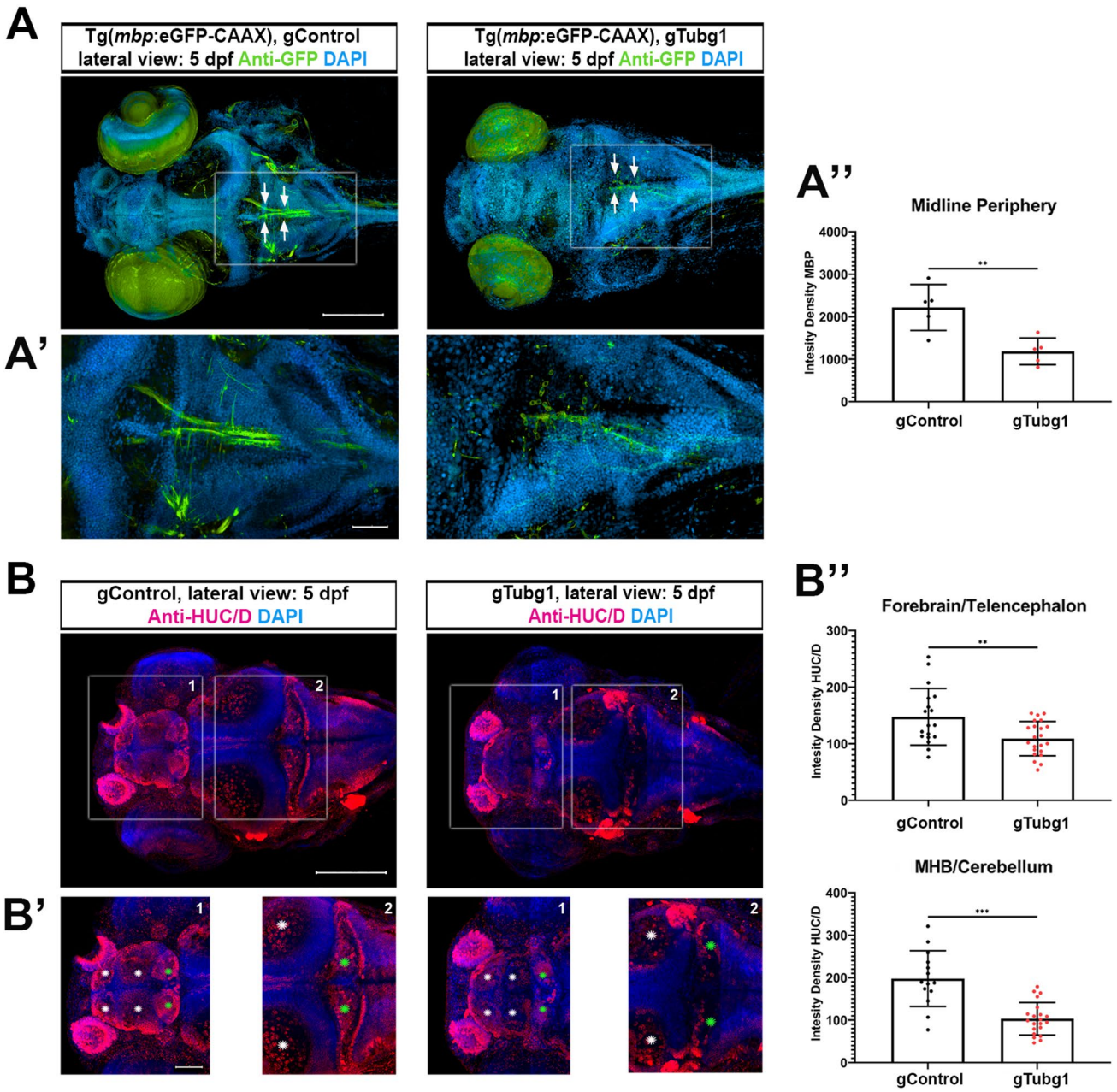

Fig. 4 *tubg1* crispants show defects in myelination and reduction in differentiated neurons. **A** The maximum intensity projections (MIPs) of anti-EGFP (green) staining of the heads of Tg(mbp:EGFP-CAAX) transgenic zebrafish larvae ($n = 12/12$ of *tubg1* crispants with a severe microcephaly) obtained from confocal microscopy reveal a decreased density of myelination decreased in *tubg1* crispants compared to the control at 5 dpf. White arrows indicate the midline periphery of the ventral hindbrain. **A'** Insets are enlarged images of the areas enclosed in rectangles in **A**. **A''** Fluorescence intensity measurement in the midline periphery region displays a significantly reduced expression of mbp in *tubg1* crispants compared to the control. **B** MIPs of anti-HUC/D (magenta) staining of the heads of zebrafish larvae ($n = 10/10$ of *tubg1* crispants with a severe microcephaly) obtained from confocal microscopy display a remarkable decrease in the amount of neuronal cell bodies in *tubg1* crispants compared to the control at 5 dpf. **B'** Insets are enlarged images of the areas 1 and 2 enclosed in rectangles in **B**. White and green labels in inset 1 indicate telencephalon and habenula, respectively. White and green labels in inset 2 indicate optic tectum and cerebellum, respectively. **B''** Fluorescence intensity measurements in the forebrain/telencephalon and midbrain-hindbrain boundary (MHB)/cerebellum regions display a significantly reduced expression of HUC/D in *tubg1* crispants compared to the control. gControl, scrambled gRNAs; gTubg1, *tubg1* gRNAs (*tubg1* crispant). Scale bars 200 µm in **A** and **B**, 50 µm in **A'** and **B'**

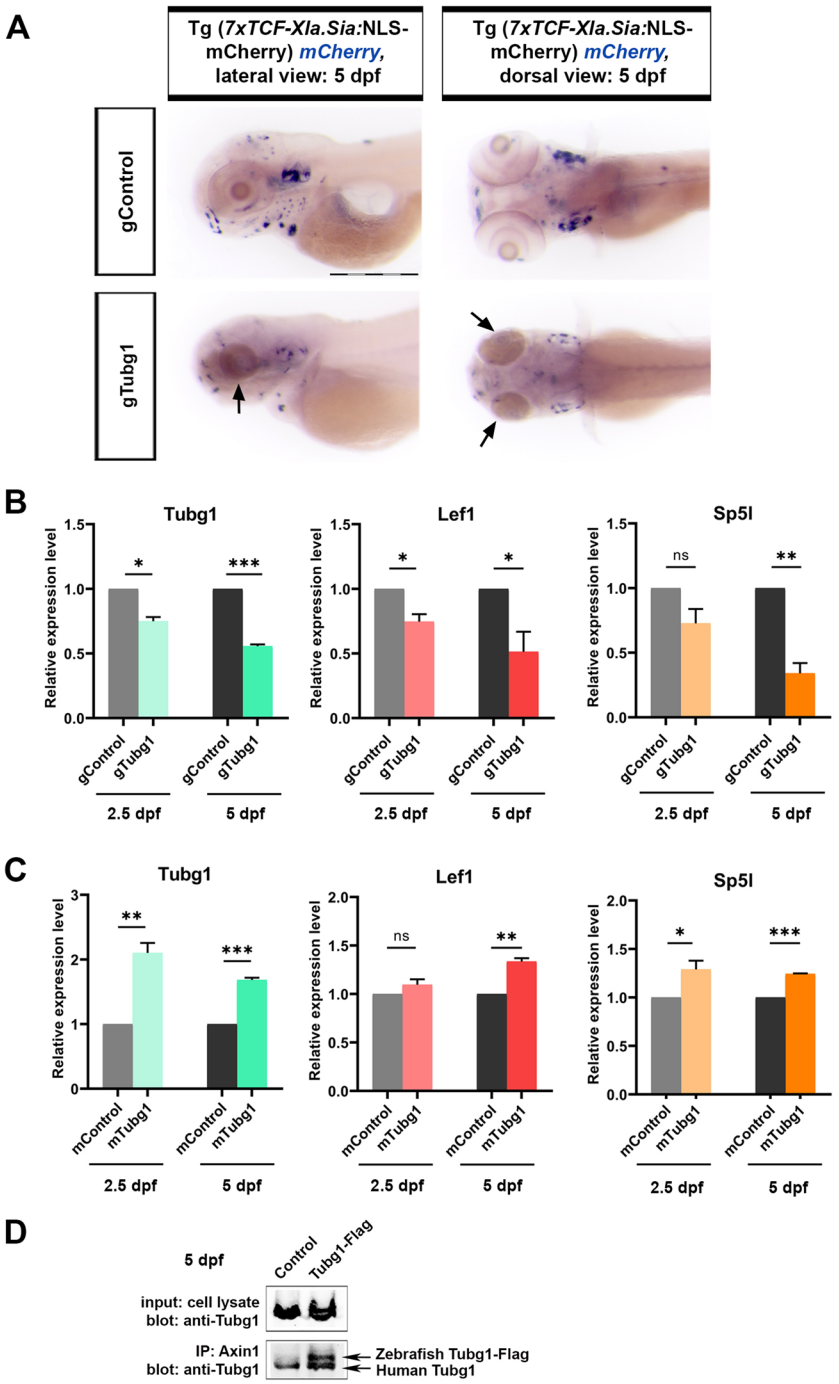

Fig. 5 *tubg1* crispants display reduced Wnt/β-catenin signaling in the head regions. **A** Whole-mount in situ hybridization for *mCherry* in Tg(*7XCF-Xla.Sia*:NLS-mCherry)[ia] transgenic zebrafish larvae at 5 dpf shows a decrease in expression domains of the Wnt reporter. Arrows indicate the reduction in eye size in *tubg1* crispants. **B** RT-qPCR on heads of *tubg1* crispants shows a decrease in expression levels of both *tubg1* and Wnt/β-catenin target genes *lef1* and *sp5l*. The relative expression levels of the genes were normalized to *rpl13a*. The fold changes in gene expression were then normalized to the control condition, which was set as the baseline with an expression level of 1. Statistical significance was evaluated using a one-sample *t*-test. $*p < 0.05$, $**p < 0.01$, $***p < 0.001$, and ns non-significant. Error bars represent ± standard deviation (SD, $n = 3$). **C** RT-qPCR on heads of larvae injected with *tubg1* mRNA shows an increase in expression levels of both *tubg1* and Wnt/β-catenin target genes *lef1* and *sp5l*. **D** Co-immunoprecipitation analysis in HEK293-T cells show that the zebrafish Tubg1 protein interacts with Axin1, a component of the β-catenin destruction complex. Please note that the endogenous human Tubg1 also interacts with Axin1. gControl, scrambled gRNAs; gTubg1, *tubg1* gRNAs (*tubg1* crispant); mTubg1, *tubg1* mRNA; gTubg1 + mTubg1, rescue group. Scale bar 1 mm

effective pharmacological treatments for patients with cortical malformations remain elusive [5, 18, 44]. Therefore, elucidating the mechanisms underlying malformations resulting from tubulin gene dysfunction represents a crucial initial step toward developing therapeutic interventions for the affected individuals. Although mammalian model organisms are commonly employed to study cortical malformations, zebrafish is emerging as a promising vertebrate model with its unique advantages in modeling syndromes associated with brain malformations. Our study introduces a novel zebrafish model with a somatic *tubg1* mutation, which reveals significant disruptions in neurogenesis and brain development, mirroring the microcephaly seen in human *TUBG1*-associated tubulinopathies. The use of zebrafish allows for detailed visualization of these developmental processes, providing insights into the dynamic changes occurring in vivo. This is particularly advantageous over traditional murine models, where such real-time observations are challenging. Furthermore, our model suggests a regulatory role of *tubg1* in the Wnt/β-catenin signaling pathway, adding

a new dimension to the understanding of *tubg1* function. The reduction in Wnt signaling activity in *tubg1*-deficient zebrafish, along with the increase in Wnt target gene expression upon *tubg1* overexpression, supports the involvement of γ-Tubulin in this critical developmental pathway. This regulatory relationship has significant implications for understanding the molecular mechanisms underlying tubg1-associated neurodevelopmental disorders. By providing a complementary tool to existing mouse and cellular models, our zebrafish model bridges the gap between in vitro studies and in vivo mammalian models and offers a practical and efficient platform for dissecting the complex genetic and molecular interactions involved in γ-Tubulin function and its role in microcephaly.

Here, we established a zebrafish model of *tubg1* (*γ-tubulin*) loss-of-function using CRISPR/Cas9 gene editing technology. Our *tubg1* crispant zebrafish larvae exhibited a significant decrease in both *tubg1* mRNA transcript and tubg1 protein levels at 2.5 and 5 dpf, confirming the loss of function. Notably, these *tubg1* crispants displayed a microcephaly phenotype reminiscent of humans with pathologic missense *TUBG1* variants associated with cortical malformations. Specifically, *tubg1* crispants exhibited reduced head size compared to the control gRNA-injected larva at 5 dpf. Interestingly, despite the γ-tubulin deficiency, body length remained unaffected, although some larvae showed a slightly curved tail phenotype.

Neurogenesis in zebrafish exhibits dynamic changes throughout embryonic and larval stages, characterized by continuous shifts in the organization and differentiation of CNS regions, as well as patterns of gene expression. Most of the central nervous system structures including the forebrain, midbrain, hindbrain, and spinal cord are defined and can be distinguished in the developing zebrafish embryo by 24 hpf [45]. Starting from 2 dpf, referred to as the early post-embryonic stage, the zebrafish brain exhibits expression patterns of essential markers of neurogenesis, closely mirroring the early embryonic mammalian brain during the initial phases of neurogenesis [46, 47]. Thus, due to the highly conserved nature of neurogenesis and the recapitulation of phenotypes seen in various human genetic disorders, zebrafish models of complex brain disorders and neurodevelopmental disorders are continually emerging (48–50). Disruption of *tubg1* function in our zebrafish crispants led to a reduction in the expression of marker genes associated with the forebrain (*neuroD1*, *elavl3*, *mag*, *gabra4*), midbrain (*prox1*, *fgf3*), hindbrain (*egr2a*, *calb2a*), retina (*prox1a*, *calb2a*), cerebellum (*calb2a*), and olfactory bulb (*calb2a*) structures. Remarkably, the brain regions affected by *tubg1* disruption align with those affected in human patients with TUBG1 missense variants or in mouse models of TUBG1-associated pathogenesis, exhibiting a broad spectrum of dysgenesis, including malformations in the cerebral cortex (forebrain), corpus callosum (forebrain), brainstem (midbrain), and the cerebellum [9, 11, 18, 51]. The clinical pathologies associated with the mutations in genes encoding tubulin isoforms manifest in various cortical abnormalities, including defective neuronal layering and a thickened cortical plate with reduced gyrification. Among these abnormalities, lissencephaly is the most severe cortical malformation [44, 52]. Notably, the phenotypic outcome in zebrafish *tubg1* crispants is reminiscent of the mutations in human *lissencephaly-1* (LIS1) gene, inducing disorganized cortical layers, hippocampus, cerebellum, and olfactory bulb in mice [2, 53].

Zebrafish *tubg1* crispants displayed a noticeable decrease in expression levels and disruptions in the expression patterns of many different neurogenesis-related genes, such as *neuroD1*, *elavl3*, *prox1a*, *fgf3*, *egr2a*, *gabra4*, *mag*, and *calb2*. Variants of human *ELAVL3* and *GABRA4* have also been associated with neurodevelopmental defects including malformations in cortical development and microcephaly [54, 55]. A de novo *EGR2* variant, producing a transcription factor with reduced capacity, has been revealed to induce severe early-onset Charcot-Marie-Tooth neuropathy and to be accompanied by white matter lesions and familial hemiplegic migraine, suggesting potential involvement of the CNS [56]. Thus, the downregulation of these genes in *tubg1* crispants implies that *tubg1* may play a crucial role in modulating the expression of key neurogenesis-related genes, thereby influencing proper brain development. Further investigation into the specific mechanisms underlying *tubg1*-mediated regulation of these genes is warranted to fully elucidate its role in neurodevelopment as well as to characterize specific types of neuronal differentiation defects and their implications in tubg1-associated neurodevelopmental disorders.

In a healthy developing brain, neuroepithelial stem cells undergo rapid proliferation and subsequently differentiate into radial glial progenitor cells (RGPCs) within the ventricular zone. While some RGPCs persist in their proliferative state, others enter a post-mitotic phase and commence radial migration along radial glial extensions [57]. This migration process is significantly influenced by tubulin mutations, which can result in alterations in cortical thickness characterized by reduced gyrus/sulcus formation. This is because microtubules play a crucial role in various neuronal processes such as radial migration, polarization, and axon initiation/growth [53, 58–61]. While we cannot definitively assert that zebrafish *tubg1* crispants exhibit lissencephaly, discernible observations reveal reduced brain sizes and structural deficits along the midbrain-hindbrain boundary, within the cerebellum, olfactory bulb, and telencephalon in zebrafish *tubg1* crispants. This could be attributed to delayed neuronal migration rather than impaired proliferation/maturation of the presumptive neurons, as indicated by our anti-HUC/D

IF results, which showed a noticeable reduction in staining intensity within the telencephalon region and a near-complete absence of staining in the hindbrain-midbrain boundary of crispants. These alterations in neuronal cell body distribution around the outer layers of the zebrafish larvae brain may suggest disrupted neuronal migration, consistent with previous studies implicating pathogenic TUBG1 missense variants that disrupt neuronal migration without affecting the proliferation of progenitor cells [51]. The *tubg1* crispant phenotype was also similar to the neuronal migration defect resulting from in vivo suppression of *tubg1* [9]. Our results have also revealed significant differences, particularly concerning myelination patterns and neuronal cell body distribution, in *tubg1* crispants compared with their healthy counterparts. We observed a notable reduction in myelination patterns at the midline periphery of the ventral hindbrain in *tubg1* crispants. These findings parallel clinical observations associated with mutations in tubulin-encoding genes, where lissencephaly patients often suffer from hypomyelination with atrophy of the basal ganglia and cerebellum. Therefore, the disruptions in myelination patterns observed in *tubg1* crispants suggest common underlying mechanisms with clinical manifestations [5, 62–64].

The Wnt/β-catenin pathway is known to play a dual role in regulating both self-renewal and differentiation in cortical neurogenesis, despite these processes typically being in direct opposition during development. Numerous studies have reported that disruption of Wnt/β-catenin signaling can result in cortical malformations due to dysregulation of both neural differentiation and neural progenitor proliferation [21, 23, 27, 65]. A clinical study documented a de novo mutation of the *CTNNB1* (*β-catenin*) gene in a patient presenting primarily with retinal detachment, lens and vitreous opacities, microcephaly, and developmental delay [66]. In the light of this information, we investigated whether Wnt/β-catenin signaling is disrupted in the *tubg1* crispant model, which exhibits a microcephaly phenotype. Our findings revealed a notable decrease in reporter expression within specific brain regions in γ-tubulin-deficient crispants, using a reporter line indicative of Wnt/β-catenin signaling. Moreover, expression levels of Wnt target genes (*lef1* and *sp5l*) were diminished in *tubg1* crispants, indirectly suggesting a decrease in the translocation of β-catenin into the nucleus. On the other hand, overexpressing *tubg1* mRNA in zebrafish embryos led to increased expression of Wnt target genes. We also found that zebrafish tubg1 binds axin1 in mammalian cells. Previous studies have demonstrated that the interaction between γ-tubulin and canonical Wnt signaling proteins can influence the localization of γ-tubulin [41, 43, 67]. A more recent study further revealed that Axin directly interacts with γ-tubulin and can recruit it to specific locations in *Drosophila* neurons [42]. While these findings underscore the regulatory role of Axin-γ-tubulin interaction in microtubule nucleation, they did not investigate the regulatory influence of γ-tubulin on Wnt/β-catenin signaling during embryonic neurogenesis. Therefore, by exploring the potential influence of γ-tubulin on Wnt/β-catenin signaling considering its reported interaction with the pathway components, our findings propose a regulatory function of γ-tubulin in canonical Wnt signaling pathway during brain development. However, the specific mechanism underlying this regulatory effect remains unclear, necessitating further studies to elucidate the molecular mechanisms through which γ-tubulin influences Wnt/β-catenin signaling. Given previous reports indicating that Axin can recruit γ-tubulin to specific intercellular locations, it is plausible that the abundance of free γ-tubulin may regulate the accessibility of Axin to the β-catenin destruction complex in the cytoplasm [42]. We speculate that γ-tubulin deficiency may lead to increased Axin participation in the β-catenin destruction complex, whereas excess γ-tubulin could sequester Axin and prevent its involvement in the destruction complex. The latter could result in the accumulation of β-catenin in the nucleus, thereby facilitating the activation of Wnt target genes. In the future, experimental designs that selectively disrupt the interaction domains of these proteins, without affecting other downstream interactions, may provide further insights into these regulatory mechanisms.

Conclusion

Our *tubg1* loss-of-function model in zebrafish recapitulates key aspects of the phenotype observed in mouse models and mirrors the clinical features seen in patients with *TUBG1* mutations. This zebrafish model not only provides a powerful and versatile system for studying γ-Tubulin function in neurodevelopment but also serves as a valuable platform for exploring human pathological variants of *TUBG1*, which cause tubulinopathies, and developing targeted therapies for these disorders. Importantly, our study is the first to investigate the impact of γ-tubulin deficiency on Wnt/β-catenin signaling during early brain development and to propose a potential regulatory role for γ-tubulin in this pathway.

Supplementary Information The online version contains supplementary material available at https://doi.org/10.1007/s12035-024-04448-2.

Acknowledgements We would like to thank Prof. David Lyons and the Aquatics Facility of The University of Edinburgh for the transgenic zebrafish line Tg(mbp:EGFP-CAAX). We would like to thank Emine Gelinci and Meryem Ozaydin from the Vivarium-Zebrafish Core Facility of IBG for providing zebrafish care, and Asli Seren from the Optical Imaging Core Facility of IBG for providing supervision for confocal microscopy.

Author Contribution GO, OC and EK designed the experiments. OC, EK, IA and EI performed the experiments. YO contributed to the interpretation of the data. OC and EK drafted the manuscript. GO edited

and finalized the manuscript. All authors read and approved the final manuscript.

Funding This work was supported by the Scientific and Technological Research Council of Türkiye (TUBITAK, grant number 217S944) and the Health Institutes of Türkiye (TUSEB, grant number 16909). GO Lab is funded by the EMBO Installation Grant (IG 3024). EK was supported by TUBITAK 2211-C Domestic Priority Areas Doctoral Scholarship Program and the Council of Higher Education (YÖK) 100/2000 Ph.D. Scholarship Program. IA was supported by TUBITAK 2210-A Master's Scholarship Program.

Data Availability No datasets were generated or analysed during the current study.

Declarations

Ethics Approval Zebrafish larvae up to 5 dpf were used in this study, which was reviewed and approved by IBG-AELEC. According to the European Commission Directive 2010/63/EU, experimentation on fish embryos at their earliest life stages is not regulated as animal experiments (https://eur-lex.europa.eu/eli/dir/2010/63/2019-06-26). This includes zebrafish embryos and early larval stages until they are free-swimming and independently feeding, corresponding to 5 dpf (days post-fertilization) when raised at 28.5 °C.

Consent to Participate and Consent for Publication This study did not involve human subjects.

Competing Interests The authors declare no competing interests.

References

1. Espinós A, Fernández-Ortuño E, Negri E, Borrell V (2022) Evolution of genetic mechanisms regulating cortical neurogenesis. Dev Neurobiol 82(5):428–453
2. Fernández V, Llinares-Benadero C, Borrell V (2016) Cerebral cortex expansion and folding: what have we learned? Embo j 35(10):1021–1044
3. Rakic P (1988) Specification of cerebral cortical areas. Science 241(4862):170–176
4. Desikan RS, Barkovich AJ (2016) Malformations of cortical development. Ann Neurol 80(6):797–810
5. Romaniello R, Arrigoni F, Fry AE, Bassi MT, Rees MI, Borgatti R, Pilz DT, Cushion TD (2018) Tubulin genes and malformations of cortical development. Eur J Med Genet 61(12):744–754
6. Barkovich AJ, Guerrini R, Kuzniecky RI, Jackson GD, Dobyns WB (2012) A developmental and genetic classification for malformations of cortical development: update 2012. Brain 135(Pt 5):1348–1369
7. Cushion TD, Dobyns WB, Mullins JG, Stoodley N, Chung SK, Fry AE, Hehr U, Gunny R et al (2013) Overlapping cortical malformations and mutations in TUBB2B and TUBA1A. Brain 136(Pt 2):536–548
8. Gungor SY, Oktay S, Hiz Á, Aranguren-Ibáñez I, Kalafatcilar A, Yaramis E, Karaca, U. Yis, E. et al (2021). "Autosomal recessive variants in TUBGCP2 alter the γ-tubulin ring complex leading to neurodevelopmental disease." iScience 24(1): 101948
9. Poirier K, Lebrun N, Broix L, Tian G, Saillour Y, Boscheron C, Parrini E, Valence S et al (2013) Mutations in TUBG1, DYNC1H1, KIF5C and KIF2A cause malformations of cortical development and microcephaly. Nat Genet 45(6):639–647
10. Romero DM, Bahi-Buisson N, Francis F (2018) Genetics and mechanisms leading to human cortical malformations. Semin Cell Dev Biol 76:33–75
11. Yuen YTK, Guella I, Roland E, Sargent M, Boelman C (2019) Case reports: novel TUBG1 mutations with milder neurodevelopmental presentations. BMC Med Genet 20(1):95
12. Oakley CE, Oakley BR (1989) Identification of gamma-tubulin, a new member of the tubulin superfamily encoded by mipA gene of Aspergillus nidulans. Nature 338(6217):662–664
13. Moritz M, Braunfeld MB, Guénebaut V, Heuser J, Agard DA (2000) Structure of the gamma-tubulin ring complex: a template for microtubule nucleation. Nat Cell Biol 2(6):365–370
14. Stearns T, Evans L, Kirschner M (1991) Gamma-tubulin is a highly conserved component of the centrosome. Cell 65(5):825–836
15. Alvarado-Kristensson M (2018) γ-Tubulin as a signal-transducing molecule and meshwork with therapeutic potential. Signal Transduct Target Ther 3:24
16. Dráberová E, Sulimenko V, Vinopal S, Sulimenko T, Sládková V, D'Agostino L, Sobol M, Hozák P et al (2017) Differential expression of human γ-tubulin isotypes during neuronal development and oxidative stress points to a γ-tubulin-2 prosurvival function. Faseb j 31(5):1828–1846
17. Bahi-Buisson NK, Poirier F, Fourniol Y, Saillour S, Valence N, Lebrun M, Hully C, Fallet Bianco N et al (2014). "The wide spectrum of tubulinopathies: what are the key features for the diagnosis?" Brain 137(6): 1676-1700
18. Brock S, Stouffs K, Scalais E, D'Hooghe M, Keymolen K, Guerrini R, Dobyns WB, Di Donato N, Jansen AC (2018) Tubulinopathies continued: refining the phenotypic spectrum associated with variants in TUBG1. Eur J Hum Genet 26(8):1132–1142
19. Thulasirajah S, Wang X, Sell E, Dávila J, Dyment DA, Kernohan KD (2022) A de novo missense variant in TUBG2 in a child with global developmental delay, microcephaly, refractory epilepsy and perisylvian polymicrogyria. Genes (Basel) 14(1):108
20. Boitard M, Bocchi R, Egervari K, Petrenko V, Viale B, Gremaud S, Zgraggen E, Salmon P et al (2015) Wnt signaling regulates multipolar-to-bipolar transition of migrating neurons in the cerebral cortex. Cell Rep 10(8):1349–1361
21. Chenn A (2008) Wnt/beta-catenin signaling in cerebral cortical development. Organogenesis 4(2):76–80
22. Da Silva F, Zhang K, Pinson A, Fatti E, Wilsch-Bräuninger M, Herbst J, Vidal V, Schedl A et al (2021) Mitotic WNT signalling orchestrates neurogenesis in the developing neocortex. Embo j 40(19):e108041
23. Kim WY, Snider WD (2011) Functions of GSK-3 signaling in development of the nervous system. Front Mol Neurosci 4:44
24. Munji RN, Choe Y, Li G, Siegenthaler JA, Pleasure SJ (2011) Wnt signaling regulates neuronal differentiation of cortical intermediate progenitors. J Neurosci 31(5):1676–1687
25. Nusse R, Clevers H (2017) Wnt/β-catenin signaling, disease, and emerging therapeutic modalities. Cell 169(6):985–999
26. Steinhart Z, and Angers S (2018) "Wnt signaling in development and tissue homeostasis." Development 145(11)
27. Buchman JJ, Durak O, Tsai LH (2011) ASPM regulates Wnt signaling pathway activity in the developing brain. Genes Dev 25(18):1909–1914
28. Kadir R, Harel T, Markus B, Perez Y, Bakhrat A, Cohen I, Volodarsky M, Feintsein-Linial M et al (2016) ALFY-controlled DVL3 autophagy regulates wnt signaling, determining human brain size. PLoS Genet 12(3):e1005919
29. Moro E, Ozhan-Kizil G, Mongera A, Beis D, Wierzbicki C, Young RM, Bournele D, Domenichini A et al (2012) In vivo Wnt signaling tracing through a transgenic biosensor fish reveals novel activity domains. Dev Biol 366(2):327–340

30. Almeida RG, Czopka T, Ffrench-Constant C, Lyons DA (2011) Individual axons regulate the myelinating potential of single oligodendrocytes in vivo. Development 138(20):4443–4450
31. Meyers JR (2018) Zebrafish: development of a vertebrate model organism. Curr Protoc Essent Labor Tech 16(1):e19
32. Kimmel CB, Ballard WW, Kimmel SR, Ullmann B, Schilling TF (1995) Stages of embryonic development of the zebrafish. Dev Dyn 203(3):253–310
33. Ye J, Coulouris G, Zaretskaya I, Cutcutache I, Rozen S, Madden TL (2012) Primer-BLAST: a tool to design target-specific primers for polymerase chain reaction. BMC Bioinformatics 13(1):134
34. Livak KJ, Schmittgen TD (2001) Analysis of relative gene expression data using real-time quantitative PCR and the 2(-delta delta C(T)) method. Methods 25(4):402–408
35. Ozalp O, Cark O, Azbazdar Y, Haykir B, Cucun G, Kucukaylak I, Alkan-Yesilyurt G, Sezgin E, et al (2021) "Nradd acts as a negative feedback regulator of wnt/β-catenin signaling and promotes apoptosis." Biomolecules 11(1)
36. Wu RS, Lam II H, Clay DN, Duong RC, Deo and S. R. Coughlin (2018). "A rapid method for directed gene knockout for screening in G0 zebrafish." Dev Cell 46(1): 112-125.e114
37. Martinez-Lopez M, Póvoa V, Fior R (2021) Generation of zebrafish larval xenografts and tumor behavior analysis. J Vis Exp 19:172
38. Sadamitsu K, Shigemitsu L, Suzuki M, Ito D, Kashima M, Hirata H (2021) Characterization of zebrafish GABA(A) receptor subunits. Sci Rep 11(1):6242
39. Planutiene M, Planutis K, Holcombe RF (2011) Lymphoid enhancer-binding factor 1, a representative of vertebrate-specific Lef1/Tcf1 sub-family, is a Wnt-beta-catenin pathway target gene in human endothelial cells which regulates matrix metalloproteinase-2 expression and promotes endothelial cell invasion. Vasc Cell 3:28
40. Weidinger G, Thorpe CJ, Wuennenberg-Stapleton K, Ngai J, Moon RT (2005) The Sp1-related transcription factors sp5 and sp5-like act downstream of Wnt/beta-catenin signaling in mesoderm and neuroectoderm patterning. Curr Biol 15(6):489–500
41. Fumoto K, Kadono M, Izumi N, Kikuchi A (2009) Axin localizes to the centrosome and is involved in microtubule nucleation. EMBO Rep 10(6):606–613
42. Weiner AT, Seebold DY, Torres-Gutierrez P, Folker C, Swope RD, Kothe GO, Stoltz JG, Zalenski MK et al (2020) Endosomal Wnt signaling proteins control microtubule nucleation in dendrites. PLoS Biol 18(3):e3000647
43. Wu Y, Jing X, Ma X, Wu Y, Ding X, Fan W, Fan M (2009) DIXDC1 co-localizes and interacts with gamma-tubulin in HEK293 cells. Cell Biol Int 33(6):697–701
44. Maillard C, Roux CJ, Charbit-Henrion F, Steffann J, Laquerriere A, Quazza F, Buisson NB (2023) Tubulin mutations in human neurodevelopmental disorders. Semin Cell Dev Biol 137:87–95
45. Schmidt R, Strähle U, Scholpp S (2013) Neurogenesis in zebrafish – from embryo to adult. Neural Dev 8(1):3
46. Kunst M, Laurell E, Mokayes N, Kramer A, Kubo F, Fernandes AM, Förster D, Dal Maschio M et al (2019) A cellular-resolution atlas of the larval zebrafish brain. Neuron 103(1):21-38.e25
47. Mueller T, and Wullimann MF (2016) Chapter 2 - Atlas of cellular markers in zebrafish neurogenesis: atlas. Atlas of early zebrafish brain development (second edition). T. Mueller and M. F. Wullimann. San Diego, Elsevier: 27–157
48. Kalueff AV, Stewart AM, Gerlai R, Court P (2015) Zebrafish as an emerging model for studying complex brain disorders. Trends Pharmacol Sci 35:63–75
49. Kozol RA, Abrams AJ, James DM, Buglo E, Yan Q, Dallman JE (2016) Function over form: Modeling groups of inherited neurological conditions in zebrafish. Front Mol Neurosci 9:55
50. Vaz R, Hofmeister W, Lindstrand A (2019) Zebrafish models of neurodevelopmental disorders: Limitations and benefits of current tools and techniques. Int J Mol Sci 20(6):1296
51. Ivanova EL, Gilet JG, Sulimenko V, Duchon A, Rudolf G, Runge K, Collins SC, Asselin L et al (2019) TUBG1 missense variants underlying cortical malformations disrupt neuronal locomotion and microtubule dynamics but not neurogenesis. Nat Commun 10(1):2129
52. Mutch CA, Poduri A, Sahin M, Barry B, Walsh CA, Barkovich AJ (2016) Disorders of microtubule function in neurons: imaging correlates. AJNR Am J Neuroradiol 37(3):528–535
53. Wynshaw-Boris A, Pramparo T, Youn YH, Hirotsune S (2010) Lissencephaly: mechanistic insights from animal models and potential therapeutic strategies. Semin Cell Dev Biol 21(8):823–830
54. Sajan SA, Gradisch R, Vogel FD, Coffey AJ, Salyakina D, Soler D, Jayakar P, Jayakar A et al (2024). "De novo variants in GABRA4 are associated with a neurological phenotype including developmental delay, behavioral abnormalities and epilepsy." European Journal of Human Genetics
55. Wang C, Zhou W, Zhang L, Fu L, Shi W, Qing Y, Lu F, Tang J et al (2023) Diagnostic yield and novel candidate genes for neurodevelopmental disorders by exome sequencing in an unselected cohort with microcephaly. BMC Genomics 24(1):422
56. Grosz BR, Golovchenko NB, Ellis M, Kumar K, Nicholson GA, Antonellis A, Kennerson ML (2019) A de novo EGR2 variant, c.1232A > G p.Asp411Gly, causes severe early-onset Charcot-Marie-Tooth Neuropathy Type 3 (Dejerine-Sottas Neuropathy). Sci Rep 9(1):19336
57. Meyerink BL, Tiwari NK, Pilaz LJ (2020) "Ariadne's thread in the developing cerebral cortex: mechanisms enabling the guiding role of the radial glia basal process during neuron migration." Cells 10(1).
58. Dupraz S, Hilton BJ, Husch A, Santos TE, Coles CH, Stern S, Brakebusch C, Bradke F (2019) RhoA controls axon extension independent of specification in the developing brain. Curr Biol 29(22):3874-3886.e3879
59. van Beuningen SFB, Will L, Harterink M, Chazeau A, van Battum EY, Frias CP, Franker MAM, Katrukha EA et al (2015) TRIM46 controls neuronal polarity and axon specification by driving the formation of parallel microtubule arrays. Neuron 88(6):1208–1226
60. Vinopal S, Dupraz S, Alfadil E, Pietralla T, Bendre S, Stiess M, Falk S, Camargo Ortega G et al (2023) Centrosomal microtubule nucleation regulates radial migration of projection neurons independently of polarization in the developing brain. Neuron 111(8):1241-1263.e1216
61. Witte H, Neukirchen D, Bradke F (2008) Microtubule stabilization specifies initial neuronal polarization. J Cell Biol 180(3):619–632
62. Hersheson J, Mencacci NE, Davis M, MacDonald N, Trabzuni D, Ryten M, Pittman A, Paudel R et al (2013) Mutations in the autoregulatory domain of β-tubulin 4a cause hereditary dystonia. Ann Neurol 73(4):546–553
63. Kumar RA, Pilz DT, Babatz TD, Cushion TD, Harvey K, Topf M, Yates L, Robb S et al (2010) TUBA1A mutations cause wide spectrum lissencephaly (smooth brain) and suggest that multiple neuronal migration pathways converge on alpha tubulins. Hum Mol Genet 19(14):2817–2827
64. Lohmann K, Wilcox RA, Winkler S, Ramirez A, Rakovic A, Park JS, Arns B, Lohnau T et al (2013) Whispering dysphonia (DYT4 dystonia) is caused by a mutation in the TUBB4 gene. Ann Neurol 73(4):537–545
65. Le Duc D, Giulivi C, Hiatt SM, Napoli E, Panoutsopoulos A, Harlan De Crescenzo A, Kotzaeridou U, Syrbe S et al (2019) Pathogenic WDFY3 variants cause neurodevelopmental disorders and opposing effects on brain size. Brain 142(9):2617–2630

66. Li N, Xu Y, Li G, Yu T, Yao RE, Wang X, Wang J (2017) Exome sequencing identifies a de novo mutation of CTNNB1 gene in a patient mainly presented with retinal detachment, lens and vitreous opacities, microcephaly, and developmental delay: case report and literature review. Medicine (Baltimore) 96(20):e6914
67. Ruan K, Ye F, Li C, Liou YC, Lin SC, Lin SY (2012) PLK1 interacts and phosphorylates axin that is essential for proper centrosome formation. PLoS ONE 7(11):e49184